Hindawi
Advances in Civil Engineering
Volume 2020, Article ID 1854813, 20 pages
https://doi.org/10.1155/2020/1854813

Research Article

Tunnelling-Induced Settlement and Treatment Techniques for a Loess Metro in Xi'an

Heng Li,[1] Enlin Ma,[1] Jinxing Lai,[1] Lixin Wang,[1,2,3] Shuoshuo Xu,[1] Ke Wang,[2,3] and Tong Liu[4]

[1]*School of Highway, Chang'an University, Xi'an 710064, China*
[2]*Institute of Geotechnical Engineering, Xi'an University of Technology, Xi'an 710043, China*
[3]*China Railway First Survey and Design Institute Group Co., Ltd., Xi'an 710043, China*
[4]*School of Science, Xi'an University of Architecture and Technology, Xi'an 710055, China*

Correspondence should be addressed to Jinxing Lai; laijinxing@chd.edu.cn and Tong Liu; liutong@xauat.edu.cn

Received 5 February 2020; Revised 7 July 2020; Accepted 19 October 2020; Published 6 November 2020

Academic Editor: Castorina S. Vieira

Techniques including pre-grouting, long pipe roof, and parameter optimization were employed to ensure the safety of loess metro tunnelling under an existing glass building. Their effects were proved through monitoring the settlement of building and surface during tunnelling. Besides, division of settlement monitoring according to processes, a new method, was conducted to control settlement in time. The highest surface settlement after construction was 16 mm only, meeting the requirement. The result indicates that it is practicable to control the tunnelling settlement strictly in extremely difficult geological areas. The settlement regularities were also studied through numerical simulation; their deformation is larger compared with in situ results while their change trends coincide during most processes. Soil excavations cause settlement primarily, accounting for more than 60%. It is suggested that dual slurry pre-grouting and process-based measurement should be employed before each excavation in water-rich loess areas.

1. Introduction

With the boom of urbanization and heavier traffic on the roads, the metro plays an increasingly important role. Metro tunnels are primarily constructed by shield method. However, limited to difficult geological environment like ground fissure area, it has to be substituted with shallow tunnelling method (STM) sometimes because the parameters of shield machine cannot change rapidly with the various soil formations. Then, some adverse consequences follow due to the disadvantage of STM method per se. After excavation, the lining support is not as timely as the shield method, so the soil will form a free surface in a period of time, resulting in excessive deformation. Because metros are usually adjacent to the surface and other structures, the deformation tends to bring hazards such as pavement cracking and building settlement. To address these questions, large numbers of studies have been conducted as follows.

Early researchers summarized the Gauss distribution of the surface settlement based on large amounts of measurement [1–5]. They are the pioneers in the regularity and prediction of surface subsidence. The subsequent development of computer technology provides convenience for numerical calculation and some specific engineering problems can be addressed in higher accuracy [6]. Nowadays with the boom of deep learning, the settlement has been studied through advanced algorithms [7]. Neural network method is more and more popular in settlement prediction [8–10]. To protect the surface building, a new formulation was put forward to calculate its subsidence [11]. Its significance lies in the fact that the formulation considered the longitudinal advance of tunnel, thus making the equivalent beam method apply in 3D model. Currently, theoretical predictions are still inaccurate because the actual information of stratum environment is difficult to obtain [12–15]. Therefore, the theoretical prediction needs to be compared

with other approaches to prove its applicability. Researchers have also studied the settlement through model tests [16, 17] and field monitoring [18–22], which increases the experience in various regions and is of guiding importance when tunnelling in similar strata. Regarding the auxiliary measures to confine settlement induced by metro tunnelling, there are three main aspects: grouting [23–28], pipe roof [29–35], and optimizing support parameters [36–40].

However, although the technology on STM comes a long way, it is still difficult to guarantee construction safety under all conditions. The subsidence is involved with many factors such as physical properties of the soil, supporting structures, and construction methods. These factors vary among different projects. It is necessary to figure out the rule of settlement in a specific environment when solving practical problems. Unfortunately, current researches on the settlement induced by shallow tunnelling and its countermeasures in loess region are not enough. In some particular situations, the settlement of buildings needs to be controlled strictly even in difficult geological strata, which requires comprehensive treatment techniques. Therefore, settlement characteristics and countermeasures in loess strata require to be further investigated.

In this study, metro tunnels were constructed under an existing building with glass exterior walls that are extremely sensitive to settlement in loess strata. To prevent potential hazards, a series of measures to control the subsidence during the construction phase were employed, including subdivision dual slurry pre-grouting, long pipe roof, and parameter optimization. Besides, a new monitoring and evaluation system was proposed which can control the settlement of each stage. All of them have achieved great success in the metro project of metro line 3 under Jinhua Hotel, Xi'an, China, as seen in Figure 1. This paper details these countermeasures and their effects were proved by monitoring. Meanwhile, a 3D numerical model was established by using Midas GTS/NX, and its result was compatible with that of field measurement. Combined with the monitoring and numerical simulation results, the subsidence characteristics were analyzed. Accordingly, reasonable proposals of pre-reinforcement in loess were herein given, leading to the establishment of a reliable reference for addressing similar engineering challenges.

2. Project Background

The section from Changlegongyuan Station to Tonghuamen Station of Xi'an metro line 3 is located on East 2nd Ring Road, Xi'an City, China, running northward and intersecting line 1. It passes some densely populated areas such as Xi'an Technological University and Tiancai Mansion. When approaching the Jinhua Hotel, the metro tunnels were constructed by STM (K32 + 135.61 – K32 + 174.94), a substitute for shield method, owing to a ground fissure near Tonghuamen Station. Above the section of STM is Jinhua Hotel which is a frame shear-wall structure with strip foundation and lime-soil compacted piles. Its exterior walls were made of reflection glass that is extremely sensitive to settlement, shown in Figure 2. The challenge of this project lies in the fact that (i) the surface building is ageing, and its external wall materials are unable to absorb large settlement; (ii) it is difficult to control the deformation in shallow tunnelling, which is easy to cause large settlement or even collapse; (iii) the project is adjacent to a ground fissure, and the soil is soft, aqueous, and unstable.

2.1. Geological Conditions. According to the geological exploration, the strata in this project are mainly low liquid-limit paleosol and paleo loess. There exists 1 m thick saturated soft loess 1.5 m above the tunnel which is water-rich (liquid index $I_L = 1.0$), plastic, and unstable. Without appropriate grouting slurry to consolidate the surrounding soil in advance, the construction disturbance may lead to hazards such as excessive subsidence or even collapse [41, 42]. The existing surface building would also be affected. The depth of groundwater is 12–14 m, changing with the seasons, and the annual variation range is about 2.0 m. The geology of the study area is given in Figure 3 and more physical and mechanical parameters of it are summarized in Section 5.1.

2.2. Construction Schemes. Bench excavation method, based on the New Austrian Tunnelling Method (NATM), means to excavate the upper section of the tunnel first and then start the excavation of the lower section. The area between the two is called bench where temporary transverse support is set. Compared with full face excavation, the bench excavation method is safer because of its smaller excavation face and less disturbance to the soils. This method has been applied in many tunnels in difficult areas in China and achieved overwhelming success. The steps of this method are shown in Figure 4.

Due to many difficulties including the poor surrounding soil and ageing glass wall, the bench excavation method was employed to meet the strict requirement of settlement (Figure 5). The tunnel includes left and right line whose section is of horse shoe shape (6.38 m width × 6.77 m height). The project was constructed with the following steps: (i) tunnelling the 9.68 m right line through the south shield hoisting hole and the north temporary dumping soil passageway; (ii) setting up the large pipe roof above the vault of 39.33 m tunnel on the left line directly; (iii) undermining left tunnel from south to north via alleyways of right line and Tonghuamen Station.

3. Techniques of Settlement Control

3.1. Subdivision Dual Slurry Pre-Grouting. Dual slurry grouting, applied in Japan first, refers to drilling by dual tube to the design depth and then grouting by utilizing a synchronous dual slurry grouting machine. The two kinds of slurry materials are A-B liquid (sodium silicate-phosphoric acid) and A-C liquid (sodium silicate-cement slurry). Firstly, the A-B liquid is used to carry out the soil drainage to improve the impermeability of the soil. Subsequently, the soil consolidation is conducted by the A-C liquid to enhance the strength and stability of the soil. The cohesive forces (c)

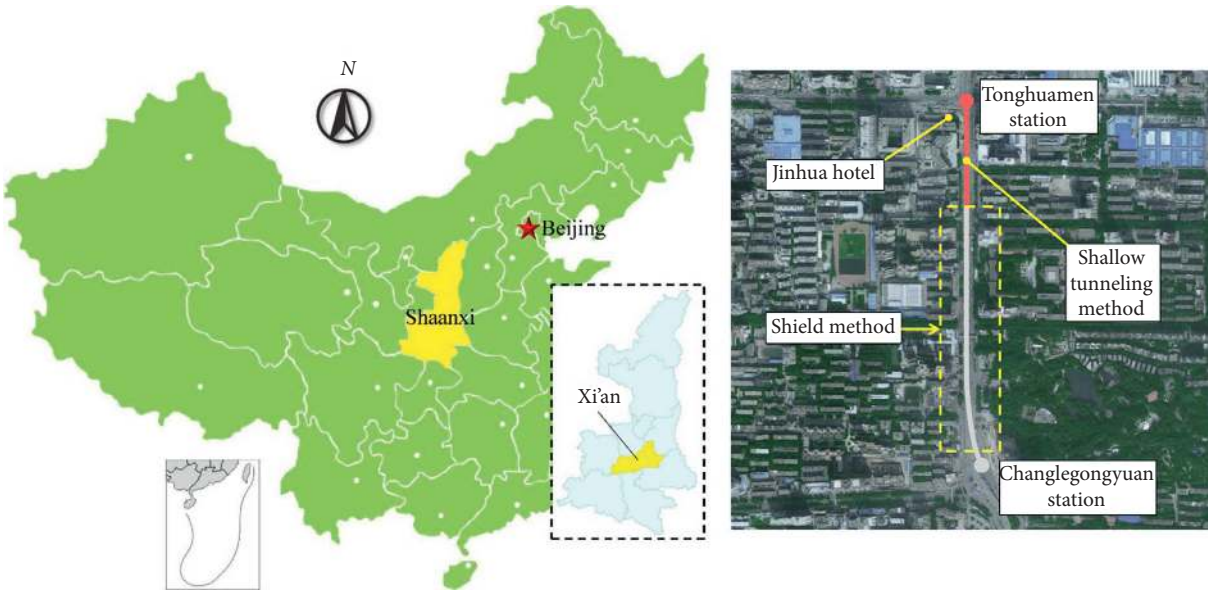

Figure 1: Location of the metro project (images by authors).

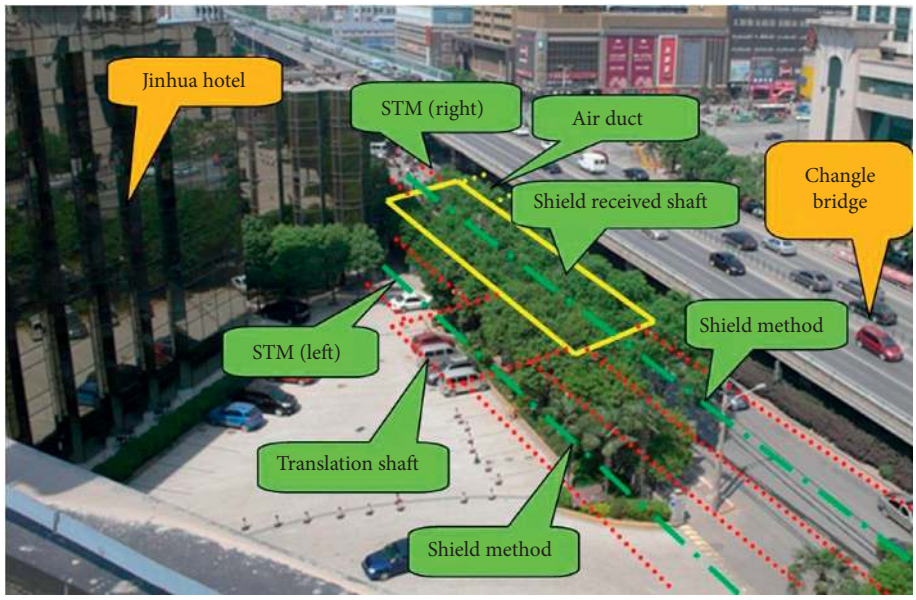

Figure 2: The relationship between the tunnel and the plane position of Jinhua Hotel building (image by authors).

and angle of internal friction (φ) are increased; the soil gets denser. After the particle gap [43] is filled with the non-flowing and consolidated slurry, the degree of permeability is reduced in the reinforced soil to form a water-repellent layer. The dual slurry grouting method has many superiorities, such as wide application areas, simple grouting equipment, and non-shrinkage slurry materials. In addition, it is economical and environmentally friendly. The components of slurry are given in Table 1.

Dual slurry grouting was introduced to this project to ensure the safety of construction by enhancing the soil 10 m behind excavation face before each excavation. The 2 m thick grouting wall was reserved when excavation is approaching the design face. Subsequently, the steel mesh was erected and the excavation face was sealed by shotcrete before the pre-grouting of next cycle. The vertical pre-grouting diagram is shown in Figure 6. Grouting includes two parts: upper section and lower section. In the process of the grouting of the upper one, there was continued excavation of the lower part to the grouting wall, followed by pre-grouting. The effect was tested by drilling sampling when the grouting had been completed. After the test result met the requirements, we moved on to next step. The site of pre-grouting is shown in Figure 7.

To modify the design and make the grouting more effective and economical, on-site observation and monitoring were carried out in time after the grouting of each cycle. We found that grouting was deficient in some areas and too

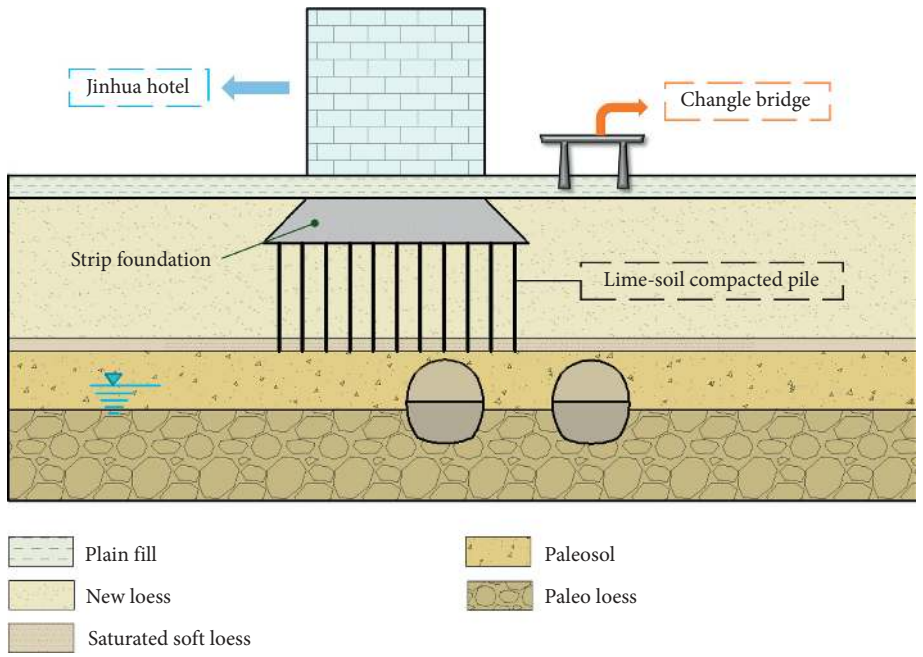

Figure 3: Vertical section of building and tunnel.

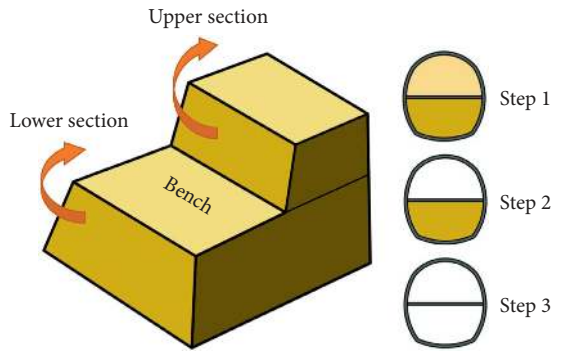

Figure 4: Bench excavation method.

(a) (b)

Figure 5: Bench excavation method: (a) upper section, (b) lower section.

much in other areas, causing both risks and waste. According to the effect of grouting reinforcement, the adjustment scheme of the next circulation grouting parameters was put forward. The original design of grouting hole was 0.6 m × 0.6 m ring to plum blossom shape. After 2 adjustments, the horizontal distance was 0.4 m, and vertical distance was 1.2 m between holes, shown in Figure 8. It enhanced the grouting effect with less cycle time. The optimization effect brought by the redesign of grouting hole

Table 1: Components of slurry.

Liquid A	Liquid B	Liquid C
Sodium silicate	Glucose	Cement
	P solution	DHP
	DHP	GOX
	GOX	XPM
Water	Water	Water

position was explained in detail in the section of surface settlement monitoring through the surface settlement curve.

After pre-grouting, the properties of soil in front of the face had been greatly improved, changing from plastic and soft plastic to elastoplastic. The cohesive forces (c) and angle of internal friction (φ) were increased, which decreased the deformation of soil into free face after excavating. The stratum deformation and surface settlement were thereby reduced. The face after pre-grouting is presented in Figure 9.

3.2. Long Pipe Roof. The pipe roof is set up above the arch of tunnel as a pre-support. The left tunnel which was the focus of this project because it is directly under the building was reinforced by a large pipe roof (diameter is 108 mm) and a battery of small grouting conduits (42 × 35 mm). Before the undermining, long pipe roof (39 m) was erected northward directly one time instead of building multiple short ones many times, which reduced the disturbance to soil so it is safer and more reliable. In addition, this method was cost-effective because it avoided setting up multiple working platforms of pipe roof. The pipe roof reinforced soil above the left tunnel; therefore, settlement above this area was controlled strictly. The top right-hand zone of shield translation shaft was taken as the working platform lest a new working place need to be established. The long pipe roof construction scheme is shown in Figure 10.

The construction procedure of the pipe roof mainly includes six steps: (1) drilling: mark the excavation contour on the working face, and mark the position of the pipe roof outside the contour according to the design requirements. All pipe roofs shall be numbered and the even holes shall be drilled first. Drill the odd holes after pipe installation and grouting to avoid hole collapse or slurry leakage. At the beginning, keep low pressure and slow rotation to control the direction, and then gradually increase the drilling speed to a steady normal pressure. When drilling, protect the pore walls with clear water to ensure the round hole, accurate angle, and enough depth. (2) Cleaning hole: use high-pressure gas to clean the drilling slag from inside to outside. (3) Pipe roof pushing and connection: install the steel pipe jacking joint sleeve corresponding to the diameter of the shed pipe on the drilling machine, align the drilling machine with the drilled guide hole, and push the steel pipe at a low speed (its impact pressure is controlled at 1.8–2.0 MPa and the pushing pressure is controlled at 4.0–6.0 MPa). Push the first steel pipe into the hole till there remains 30–40 cm outside, and then start the drilling machine to reverse, so that the jacking joint sleeve can be separated from the steel pipe. In order to avoid that, the number of joints in the same cross-section is not more than 50%; the first pipe and the last pipe are adapter pipes when the middle one is a standard section. Pipe jacking shall be carried out in time after hole forming to prevent hole collapse from affecting pipe jacking. (4) Sealing the gap: to ensure the grouting quality, after the installation of the steel tube, the gap between the steel tube and the pore wall shall be sealed with hemp thread and anchoring agent. Before grouting, a grout-stopping plug shall be set at the orifice and a tee joint shall be installed on the grouting pipe orifice. (5) Pre-grouting: the material used for grouting is cement slurry, whose water-cement ratio is 1 : 1, and the grouting is carried out from top to bottom at the arch. Its initial pressure is 0.5–1.0 MPa and the final pressure is 2.0 MPa. The grouting is stopped after holding the pressure for 15 min. Generally, the grouting volume is 1.5 times that of the drilling cylinder. When the grouting volume exceeds the limit and fails to meet the pressure requirements, the slurry concentration shall be adjusted to continue grouting until it meets the grouting quality standards, so as to ensure that the pores around the drilling rock and steel pipe are filled with slurry, and then the grouting can be terminated. (6) Sealing grouting hole: after grouting, use M7.5 mortar to seal the orifice in time.

During the pipe roof setting, the following two key points need attention: (1) grouting holes should be drilled on the pipe roof before setting; (2) the pipe roof is strictly constructed based on the design position, and it is forbidden to be intruded within the boundary line of tunnel. Relevant construction parameters are given in Table 2 and the construction process is presented in Figure 11.

3.3. Optimization of Support Parameters. Regarding the challenge in underground construction, the conventional method is primarily strengthening the structures in highly risky places, such as thickening lining and reinforcing steel. This method does ensure the safety of structures, but aimless reinforcement obviously increases costs and time. In this project, according to the characteristics of this project, based on experience, numerical simulation, and field test, the support performance of the arch foot and the pre-grouting of the arch were selectively strengthened in the left tunnel near the building. There are three specific optimizations: (1) in order to control the settlement of the initial support in the upper section, I-steel large arch foot was added to the grid bottom of the upper section to decrease the settlement of the arch foot; (2) during the tunnelling in the vicinity of the building, the number of pin locking anchor pipes was increased from two to three in each grid, thereby strengthening it; (3) the number of conduits was increased under the building, and their longitudinal distance was decreased from 1.5 m to 1.0 m.

One of the key processes is the installation of large arch foot. During the installation of the grid in the upper tunnel, the light U-steel mat was used under the grid arch foot to increase the stress face between the grid arch foot and soil, thereby reducing the settlement of the steel grid. During the excavation of the lower part, the light U-steel mat was

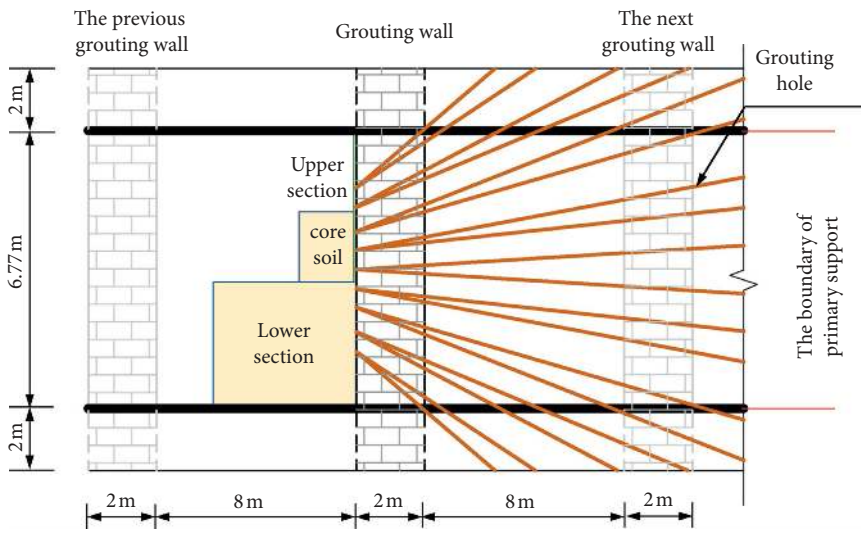

Figure 6: Pre-grouting vertical diagram.

Figure 7: In situ grouting equipment and environment.

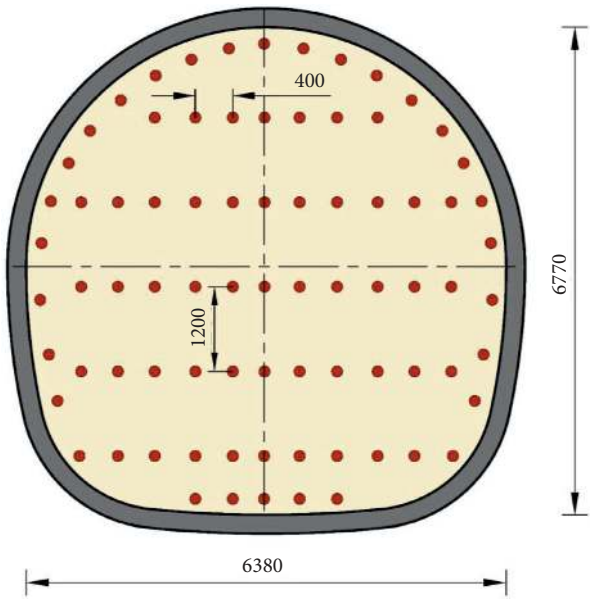

Figure 8: Grouting holes distribution after adjustment (mm).

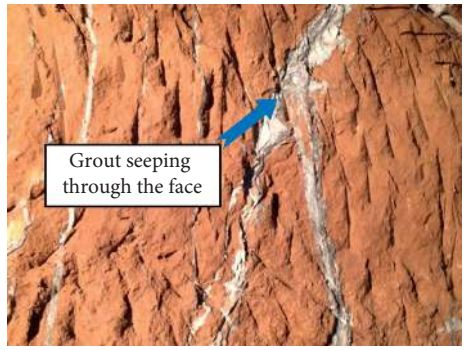

Figure 9: Grouting effect.

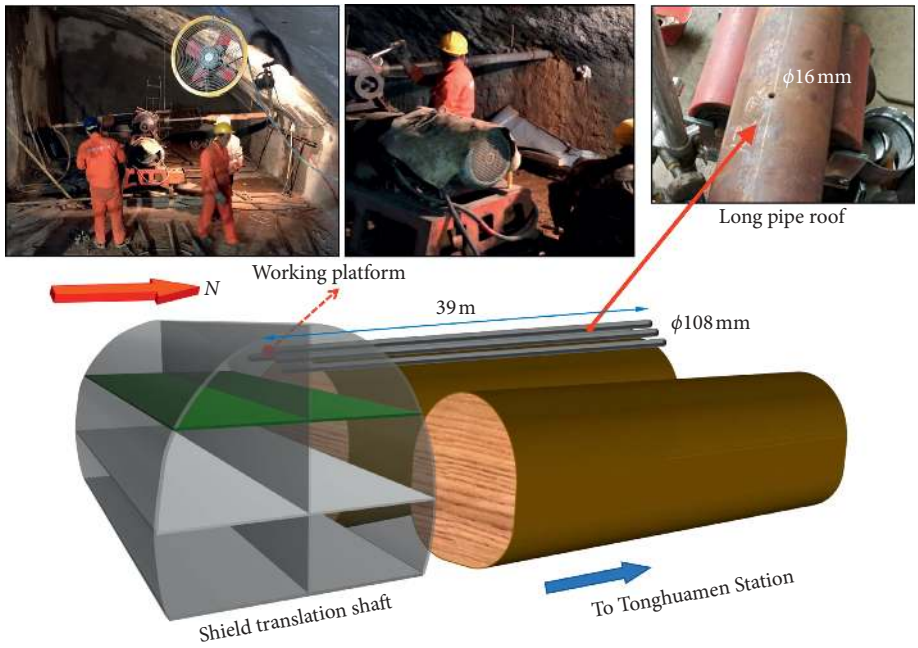

Figure 10: Sketch map of long pipe roof setting.

Table 2: Parameters of pipe roof.

Item	Parameters
Pipe diameter	108 mm
Distance between pipes	0.35 m
Setting angle	1–2°
Pipe thickness	5 mm
Diameter of grouting hole	16 mm
Distance between holes	15 cm
Initial grouting pressure	0.5–1.0 MPa
Final grouting pressure	2.0 MPa
Grouting time	15 min

removed and the connecting plates of the upper and lower steel grids were linked firmly by bolts. The relationship between the grid bottom and the light *U*-steel mat is shown in Figure 12.

Another crucial process is that, after the installation of the grid steel frame, the anchor pipe for locking foot shall be set near the bottom of the grid. An anchor pipe was added at one side of each grid when the section is near the building. A U-shaped steel was installed above the pipe head, which was close to and welded firmly with the head of the anchor pipe, thereby forming them into an integrated structure, as shown in Figure 13.

3.4. Division of Settlement Monitoring according to Process. Monitoring is an important process of NATM. Design parameters are modified by comparing measured deformation with expectations. Currently, however, there is usually only one total limit to guide the construction in underground engineering, which requires experienced engineers to judge the structural safety according to the distance between the measurement results and limit. This is unreliable because even though the deformation has been excessive at a stage, it cannot arouse the engineers' vigilance if the total deformation is normal. It would be too late to take any effective measures once the abnormality was not found in time, causing serious engineering hazards.

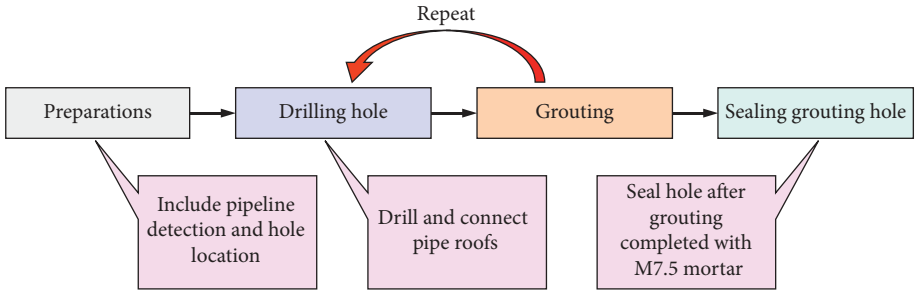

Figure 11: Process of long pipe roof setting.

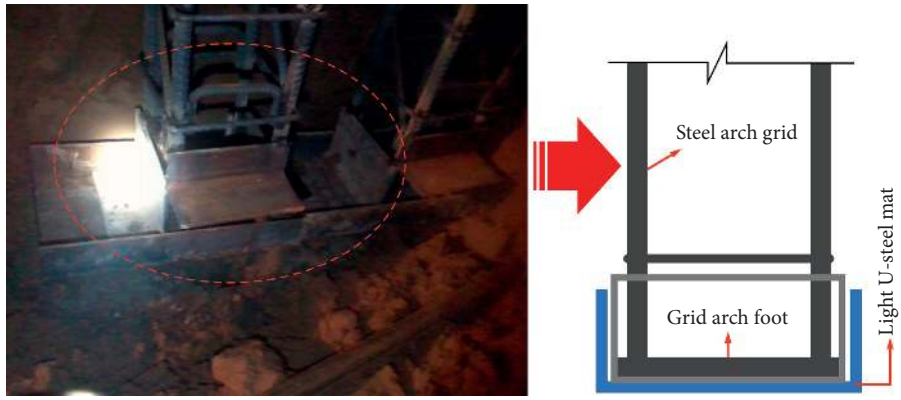

Figure 12: The setting of light *U*-steel mat under the bottom of the steel arch.

Figure 13: Connection of lock pin anchor pipe on-site.

Table 3: Limit subsidence of each process.

Process	Proportion (%)	Limit subsidence (mm)
Long pipe roof setting	+5	+1
Pre-grouting	+5	+1
Upper excavation	−50	−10
Lower excavation	−35	−7
Second lining	−15	−3
Post-construction	−10	−2
Total	−100	−20

Division of settlement monitoring, a new method, was proposed to address the above problems. It refers to dividing the total subsidence limit into each part according to their influence on settlement. As a result, we can control subsidence within the limit value in every step. The main factors that could influence the subsidence are the following: (a) pipe roof setting: it may change the local soil moisture content and density; (b) dual slurry pre-grouting: it may cause deformation with improper operation; (c) excavation: it will cause the soil stress redistribution and bring subsidence before the stress rebalance of the soil; (d) soil consolidation: it will cause subsidence during excavating; (e) gap between primary lining and soil: it will certainly cause the subsequent subsidence; (f) in second lining construction, removal of temporary bracing will change the internal force of primary supporting and cause its deformation further. In view of the six factors and engineering experience, the allowable subsidence (20 mm) was divided into six relevant processes, as shown in Table 3.

Specifically, the settlement or uplift induced by the above six independent construction processes will be counted separately, and the settlement induced by alternate steps such as grouting and excavation will be accumulated. This method was applied in the subsidence monitoring and controlled it well in every process of construction, showing a great advantage.

4. Monitoring Results and Discussion

4.1. Building Settlement Monitoring. Jinhua Hotel is the focus of this measurement. The monitoring points are placed along the east, west, and north sides of the exterior walls to control building settlement in time (Figure 14). The historical settlement curves were drawn from four typical measuring points, as shown in Figure 15. The settlement increased about 13 mm from the beginning of metro construction. There were several slight rises which were caused

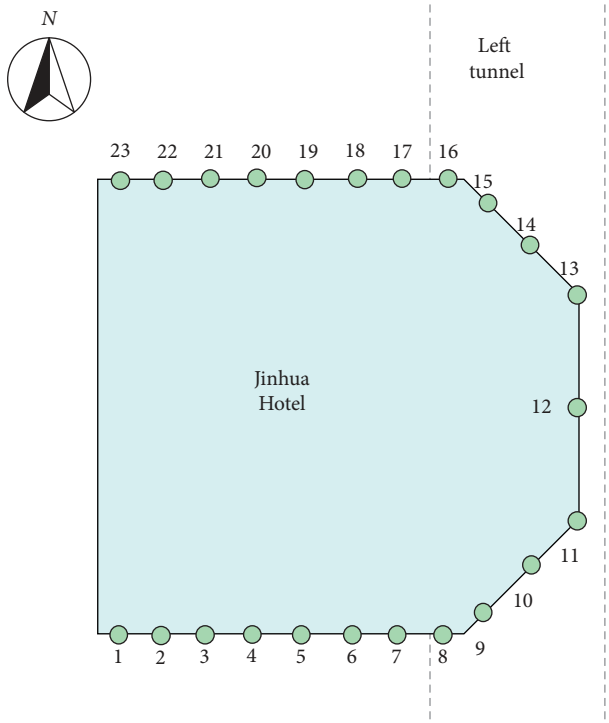

Figure 14: Building subsidence monitoring points.

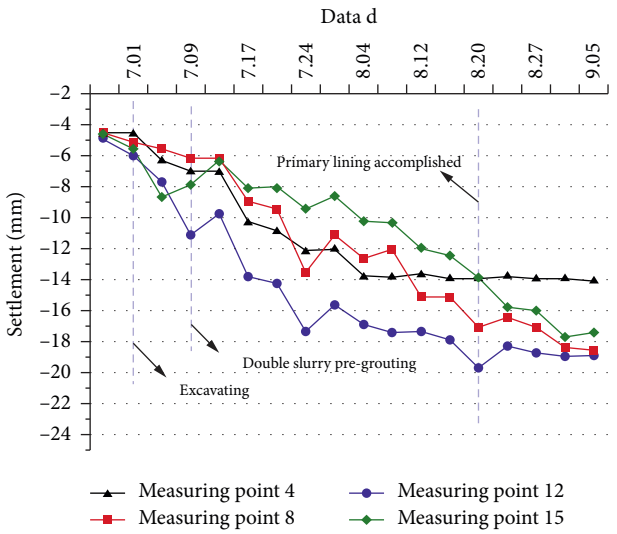

Figure 15: Building subsidence curves.

by pre-grouting. The building had already subsided about 4 mm before excavation, which was induced by previous construction, making it even harder to ensure the structural safety. When the tunnel was excavated, the subsidence increased gradually and had not been stable until the completion of the initial support. Compared with the other three points, point 15 did not change obviously in the first half of the whole construction process, which was mainly concentrated in the latter part, consistent with the sequence of the construction stage.

The settlement distribution after construction can be drawn according to the accumulative settlement of each measured point of building, as shown in Figure 16. The east wall near the tunnel is obviously decreased, and the settlement value is about twice that of other walls. The maximum was 18.9 mm; the minimum and differential subsidence were 10.4 mm and 8.5 mm, respectively; the inclination is 8.5/32000 = 0.265‰ < 3‰, satisfied on the basis of the code for design of building foundation in China (Table 4). It is very difficult to achieve such a result when building metros by using underground excavation in water-rich loess areas. Therefore, the treatment techniques introduced are effective.

4.2. Surface Settlement Monitoring. The measured points were arranged along the edge of the building within 25 m from the tunnel center line, which is from north to south (Figure 17). Several typical points were selected and their settlement curves are drawn in Figure 18. It can be seen that settlement along the tunnel has little difference (2–4 mm). The overall trend of these points is downward, with several rises during the process. The surface settlement has been up to 4–8 mm before excavation which was caused by previous construction nearby, increasing the difficulty of subsidence control. With the disturbance regarding excavation, the surface subsidence was further increased. Thereafter, there were several obvious rises of 2-3 mm, which coincided with the grouting time, indicating that it has mitigation and inhibition effect on settlement. Since 20th August, the rate of subsidence has slowed down. The subsequent settlement is only 1-2 mm, accounting for 10%. Therefore, later construction steps (e.g., pouring secondary lining) did not affect the surrounding soil notably after the primary lining was accomplished. The structure tends to be stable gradually. During the whole construction process, the maximum surface subsidence is about 16 mm, less than the control limit of 20 mm, which proves the effectiveness of the reinforce measures.

On 13th July, all points on the surface had risen sharply. Among them, points 5–3 and 4–3 that are close to Jinhua Hotel were the most intense. This was caused by the pre-grouting pressure under the building. Obviously, uplift offsets part of the settlement. However, an excessive rise is also not conducive to security, especially when the change is relatively rapid. The layout of this grouting hole is quite unreasonable, which leads to excessive grouting and unnecessary waste, and the surface uplift caused by it is dangerous. Therefore, the plane design of pre-grouting holes was optimized after this time, as introduced in Section 3.1. It can be found that, after 13th July, the pre-grouting did not cause large-scale surface uplift, showing that the hole position optimization is very effective.

4.3. Tunnel Deformation Monitoring. After the left tunnel had been completed, its vault displacement and clearance convergence were measured, shown in Figure 19. The measurements were conducted per 5 m longitudinally, including eight tunnel cross-sections totally. Figure 20 compares the vault settlement and clearance convergence of each section and shows the relative position relationship between each section and Jinhua Hotel also. It can be seen that the

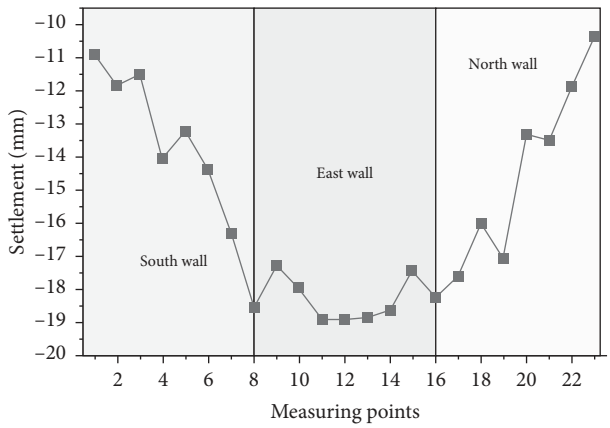

Figure 16: Building subsidence distribution.

Table 4: Allowable values of buildings foundation deformation.

The subsidence of multi-storey and high-rise buildings	Hg ≤ 100 m	200 mm
The overall inclination of multi-storey and high-rise buildings	24 m Hg ≤ 60 m	0.003

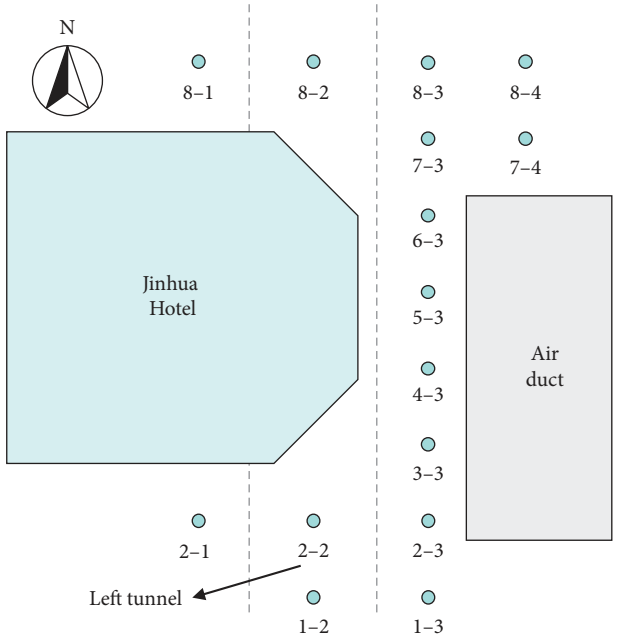

Figure 17: Surface subsidence measuring points.

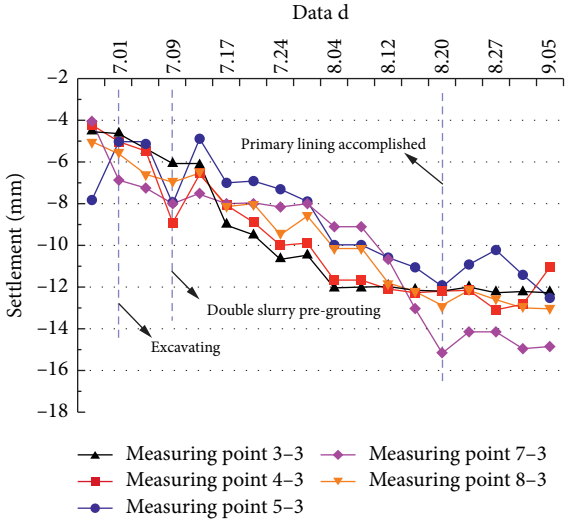

Figure 18: Surface subsidence curves.

deformation of left tunnel is not uniform in the longitudinal direction and it peaks in the vicinity of the intersection of the left line and the building. Normally, the vault settlement is consistent with clearance convergence, but there are two anomalies in Figure 20: one is that the vault settlement of the fifth section was very small, which is probably due to the strict and sufficient grouting over the tunnel in this area; the other is that the clearance convergence was too high in the 8th section and at the same time we noticed that the settlement of measuring point 8-3 in Figure 14 was also large, which is exactly above the 8th section, indicating that it may be caused by the negligence of construction or the sudden strata change. Overall, the structure was stable.

Comparing Figures 12, 14, and 15, the maximum settlement values of building, surface, and left tunnel are about 19 mm, 15 mm, and 8 mm, respectively. They all occurred near the building and left tunnel. The difference between the settlement of the tunnel vault and the ground surface is about 7 mm. Considering that the distance between the two is close to 10 m, it can be considered that the relative deformation of the stratum soil is very small. Therefore, the soil consolidation settlement is little because of the sealing-up effect of pre-grouting.

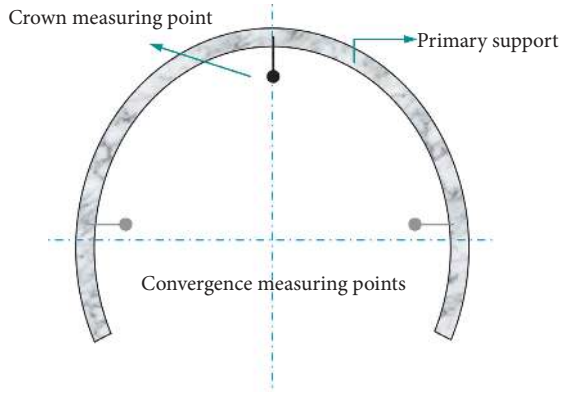

Figure 19: Tunnel deformation measuring points.

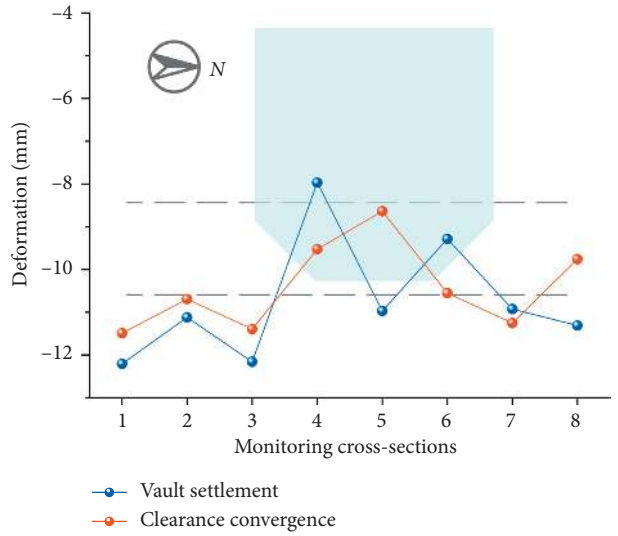

Figure 20: Longitudinal tunnel deformation distribution.

5. Numerical Simulation

5.1. Finite Element Model. To better study the grouting effects and settlement regularity of the existing buildings in the loess area, a three-dimensional model is established using Midas GTS/NX, which contains 5 layers of soil according to the geological prospecting data. The thickness of each layer is 1.2 m, 7.6 m, 1.0 m, 4.2 m, and 15.0 m, respectively. The two tunnels are both 10 m deep with horseshoe section (width 6.40 m × height 6.80 m). The size of Jinhua Hotel is 32 m × 25 m × 21 m (length × width × height). Figure 21(a) shows the overall finite element model and Figure 21(b) illustrates the pre-grouting model which simulates the process of diffusion grouting of each stage based on the face before excavation. Figure 21(c) demonstrates the foundation under the building. The green grids simulated the foundation after lime-soil compaction pile treatment, and the yellow grids simulated the strip foundation at the bottom of the building.

Referring to the geological prospecting, the parameters of soil layer were determined according to the elastic-plastic theory. The building materials (C30 concrete) and tunnel support parameters were determined based on the elastic theory and practical experience. Referring to the design standard of metro tunnel and realistic design data in this construction, the parameters of shotcrete layer, grouting materials, and anchor bolt were determined. The detailed parameters are shown in Table 5.

The finite element model satisfies the following assumptions: the stress-strain characteristics of each soil layer obey the Mohr–Coulomb criterion. The building, foundation, anchor bolt, and grouting body meet the elastic deformation characteristics. All materials are homogeneous, continuous, and isotropic. Among them, Jinhua Hotel is simplified as a four-span frame structure, with beam element for the column, plate element for the floor, and beam element for the strip foundation. Anchor bolt was simulated by embedded beam element; initial support (shotcrete) and pipe shed of tunnels were established by plate element. The others were simulated by 3D solid elements. The original stress only considers the self-weight stress of soil and buildings. The horizontal displacement on four broadsides is constrained and the bottom elements are all fixed. The numerical simulation includes two construction conditions:

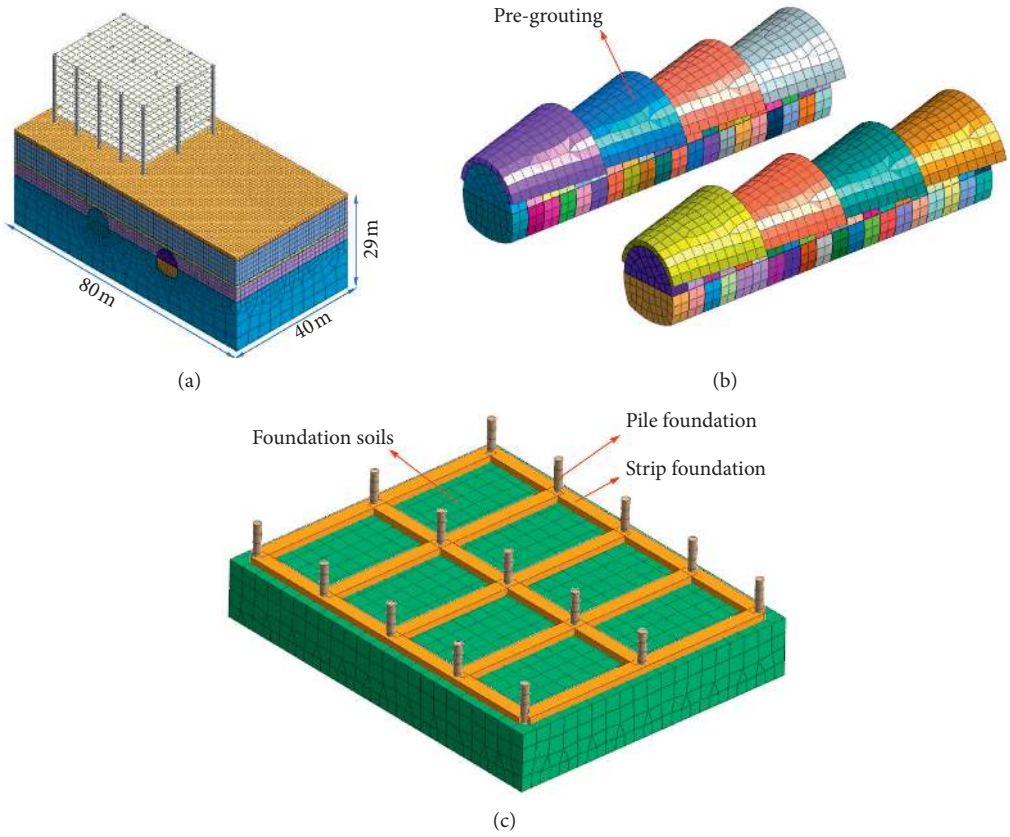

Figure 21: The finite element models: (a) overall model, (b) grouting model, and (c) building foundation model.

Table 5: Physical and mechanical parameters.

Materials category	γ (kN·m^{-3})	E (MPa)	μ	C (kPa)	φ (°)	Lateral pressure coefficient
Plain fill	16.5	6.0	0.37	10	10	0.7
New loess	19.3	6.5	0.33	27	17	0.5
Saturated soft loess	19.8	5.5	0.33	30	17.5	0.5
Paleosol	19.5	7.0	0.33	31	17.5	0.5
Paleo loess	20.2	8.0	0.33	36	18.3	0.5
Foundation	30.5	150.0	0.35	40	25.5	0.7
C30 concrete	24.0	3.0×10^4	0.2	—	—	—
Shotcrete	22.0	2.5×10^4	0.2	—	—	—
Grouting materials	21.0	1.2×10^2	0.3	—	—	—
Pipe shed	78.0	2.0×10^5	0.3	—	—	—
Anchor bolt	78.5	2.1×10^5	0.3	—	—	—

non-grouting and pre-grouting. The construction steps were simulated based on the actual construction. The whole construction process can be divided into four cycle steps: (1) pre-grouting (empty step in non-grouting condition), (2) excavating the upper soil, (3) supporting the upper part, and (4) excavating and supporting the lower part. According to the time factor of the construction sequence, the stress induced by the upper excavation is loaded into the four stages by the load release coefficient of 10%, 10%, 60%, and 20% while the release ratio of the lower excavation is 10%, 10%, 10%, and 70%, respectively (loads not released in the last step are released in one time). The three-dimensional excavation model is properly simplified to simulate the construction process, shown in Figure 22.

5.2. Building Settlement

5.2.1. Variation Regulations along with Excavations. According to the results of numerical calculation, the deformation regularities of columns are similar in north-south direction. Therefore, the bottoms of 5 columns in the middle of the building were selected as the research object (Figure 23), and their settlement curves during the simulation process can be obtained. Figures 24 and 25 compare the settlement curves of the two construction conditions (non-grouting and pre-grouting).

The building presents a continuous settlement trend during the construction. The maximum cumulative settlement occurs at point 4, nearest to the left tunnel, which is

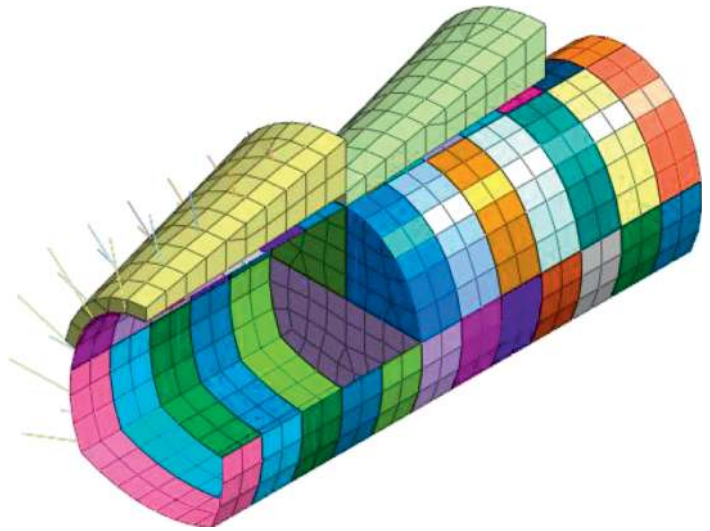

(a)

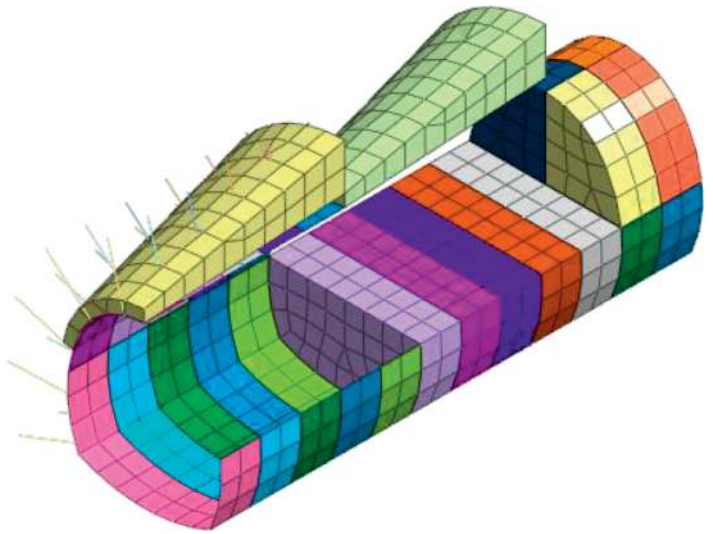

(b)

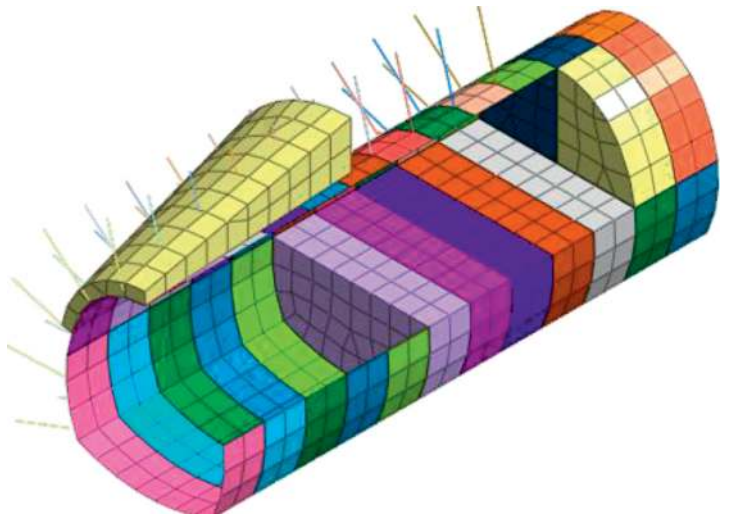

(c)

Figure 22: Continued.

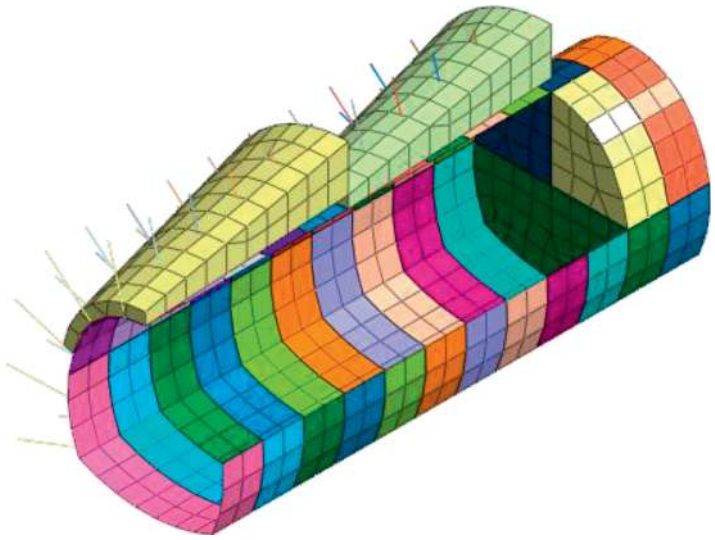

(d)

Figure 22: Simulation of underground tunnelling construction: (a) pre-grouting, (b) excavating the upper soil, (c) supporting the upper part, and (d) excavating and supporting the lower part.

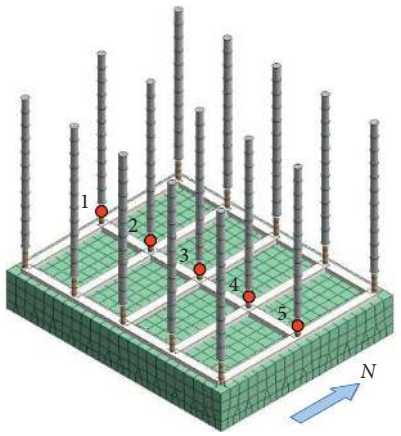

Figure 23: Schematic map of measuring point.

119.50 mm and 16.50 mm, respectively, in the two conditions. Compared with the condition of non-grouting, the maximum subsidence with grouting is reduced by 86.2%, which confirms that the pre-grouting is highly effective in loess to control the subsidence during tunnelling. Points 1 and 2 are nearly steady due to the far distance from the construction site, revealing the general influence boundary of this tunnelling project on the surface structures. The subsidence of each point is negatively related to the distance from the center line of the left hole, causing the building to incline towards it, and the differential subsidence value reaches 110 mm finally without grouting. The local grouting greatly stabilizes nearby points 4 and 5, highly dwindling the overall inclination of the building. It is noteworthy that the excavation of the right line has little impact on Jinhua Hotel, which accounts for less than 15% of the total. With the left line construction, the subsidence of buildings increases sharply. Take point 4 as an example (Figure 24); if the excavation footage is 2m per day, the subsidence rate will reach 4.33 mm/d without grouting, which occurs at the beginning of the left excavation while the maximum deformation occurs after all the soil under building is excavated. At the same time, the subsidence decreased slightly after the tunnelling passes through the building because the support structure on the north side of the building has formed an extrusion effect on the subsoil, prompting it to move southward, and thus restraining the settlement.

Comparing the deformation curves of field measurement (Figures 15 and 16) and numerical simulation (Figure 25), it can be seen that numerical simulation has more accurate results in regularity analysis. However, as for the specific deformation values, it is quite different from the practical measuring results, which is mainly because the real environment and construction conditions cannot be completely simulated by the finite element model. The numerical model has to be simplified to calculate, but this simplification must be selective. It cannot be simplified on the key issues that have great impacts on the results, such as the existing

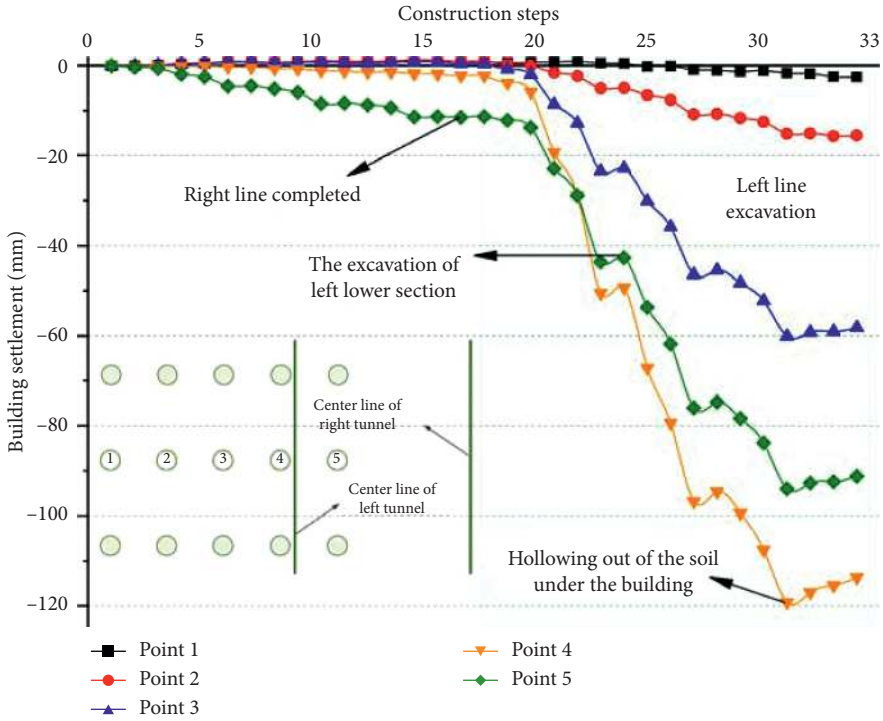

Figure 24: Building subsidence curves (non-grouting).

buildings on the surface in this model. Some other auxiliary facilities, by contrast, should be simplified. The simulation results are consistent with the actual results in law, so that numerical simulation can also contribute to the division of settlement monitoring.

5.2.2. Distribution after Construction. The building subsidence distributions of the two conditions are obtained through numerical simulation, as shown in Figure 26. The maximum settlement of the building happens exactly above the left line and its longitudinal difference (north-south direction) is tiny. Obviously, grouting greatly reduces the settlement of the building and the decrease is more apparent near the left tunnel because the grouting is also concentrated in this area. It can be noticed that there was discontinuity in subsidence between the strip foundation and soil which indicates the deformation of foundation soil was not completely transmitted to the building structure, manifesting the ability of structures to resist deformation.

To further analyze the settlement distributions, the final displacement of building bottom in two conditions along horizontal direction was drawn, as shown in Figure 27. The subsidence of the building is centered on the left line ($x = 0$), with a skew L type distribution, which has a long and gentle left side and a short and steep right side. Besides, there exists a slight uplift on the left about 0.99 mm and 0.30 mm in two conditions, respectively. The longitudinal differential subsidence of the building is not significant. The disturbance of tunnelling is mainly concentrated within 15 m (2.5 times tunnel diameter) from the left center line—the disturbance range. This result also implies that the right tunnelling almost did not influence the building due to the far distance (18 m). Without grouting, the maximum subsidence of the building is 119.5 mm and the maximum difference is 120.5 mm. Thus, the inclination is $120.5/32000 > 0.003$, which does not meet the requirements (Table 4). When the soils are pre-grouted before each excavation, the settlement decreases notably due to the strengthening of deformation modulus of soils, whose self-stability is increased heavily. Moreover, the closer to the tunnel, the more effective the subsidence containment will be, which reduces the differential subsidence greatly.

5.3. Distribution of Surface Settlement. The surface displacement is ineluctable during the undermining, which will affect the traffic on the road and surrounding buildings so we should study its distribution form in order to reinforce the dangerous areas and prevent potential disasters. Figures 28 and 29 compare the cumulative settlement on surface in the two conditions. Their distributions are similar in two aspects: (1) the settlement range is approximately 1.2–1.5 times that of the construction area. (2) The whole ground is distributed in the oblique W type and the left subsidence grooves are deeper than the right due to the buildings. Without grouting, the displacement is mostly more than 40 mm in settlement range, and the groove is deep, reaching 142.5 mm, which has not met the requirement. The subsidence values dropped rapidly under condition of pre-grouting, the maximum of which is only 31.3 mm, and the groove becomes gentle, which is favorable for the surface buildings and road traffic. Therefore, the pre-grouting before each excavation is suggested. In addition, the slurry quality

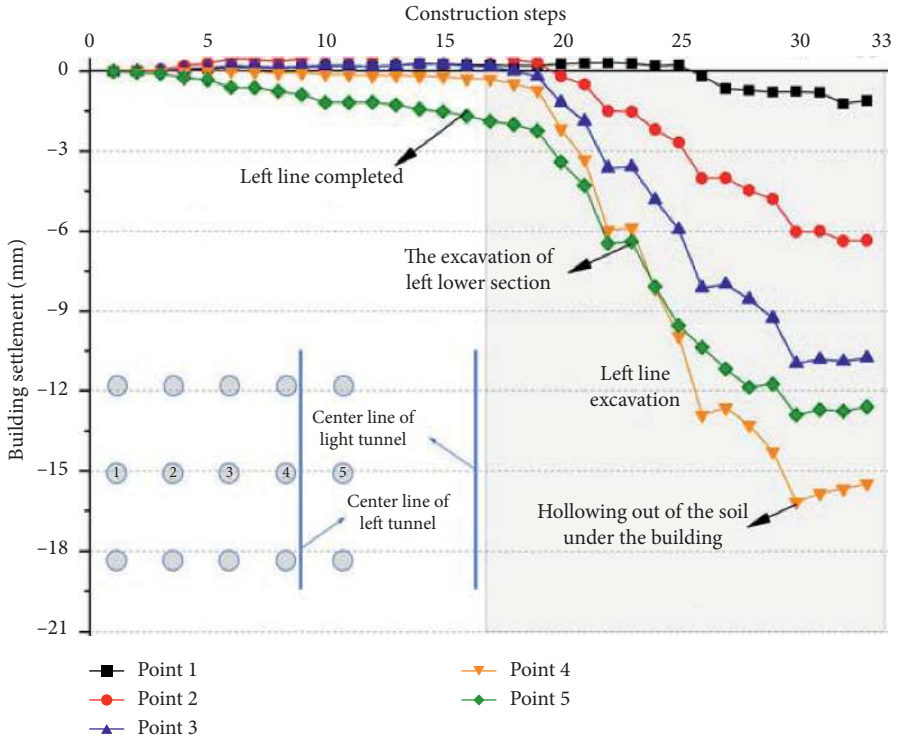

Figure 25: Building subsidence curves (pre-grouting).

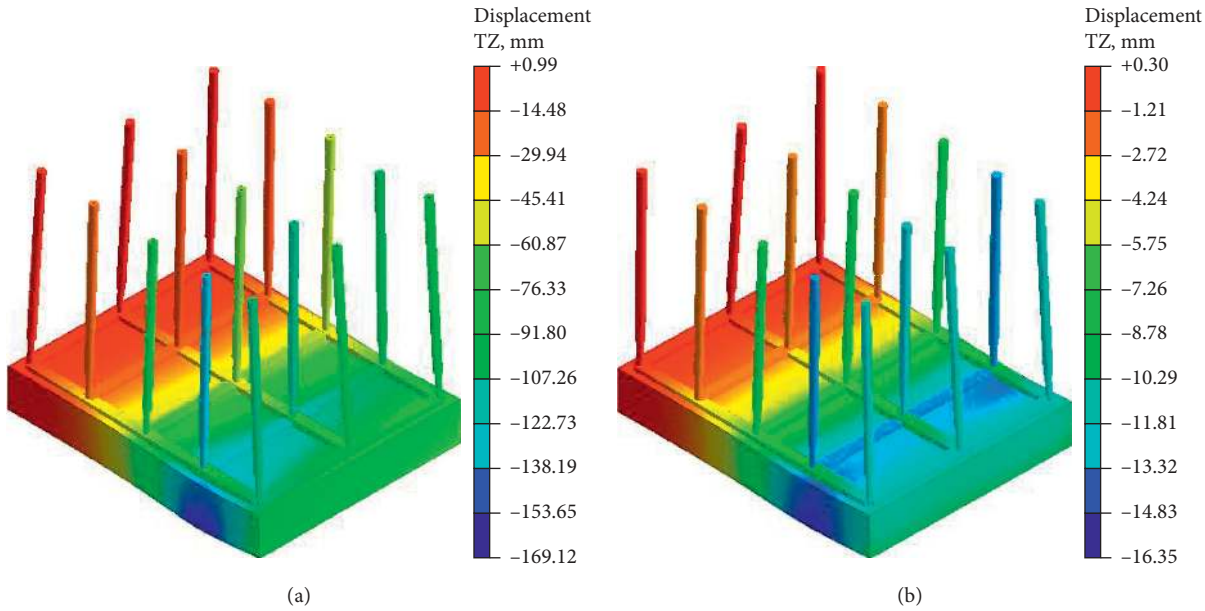

Figure 26: Vertical displacement distribution of building after construction: (a) non-grouting, (b) pre-grouting.

and grouting range should be guaranteed to enable less loss of the strata.

Compared with the results measured in the field, we have to admit that numerical simulations cannot reflect the actual situation. Therefore, currently we mainly rely on monitoring to identify the structure states to ensure the safety of underground construction [44–46]. However, numerical simulations perform well in regularity analysis [47–55]. In this case, the surface settlement curves obtained by simulation are consistent with the practical trend, although its values are quite different from the real situation. Thus, we can predict the influence extent of different construction procedures on the surface settlement in advance. The method of controlling settlement by the process proposed in

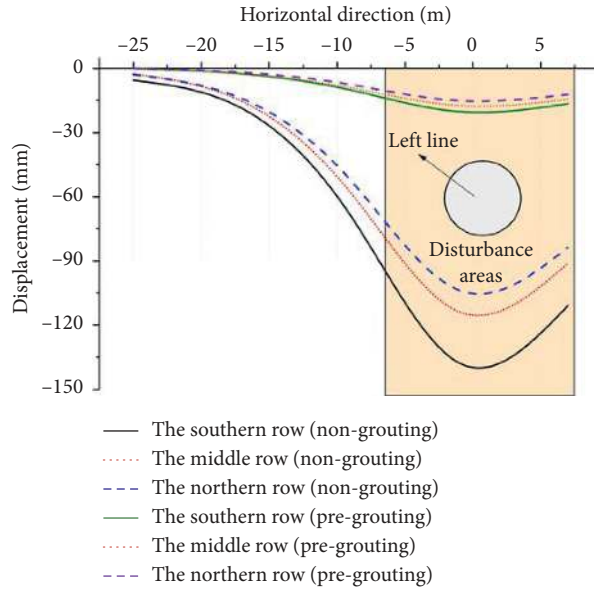

Figure 27: Simulated displacement distributions of building foundation after construction.

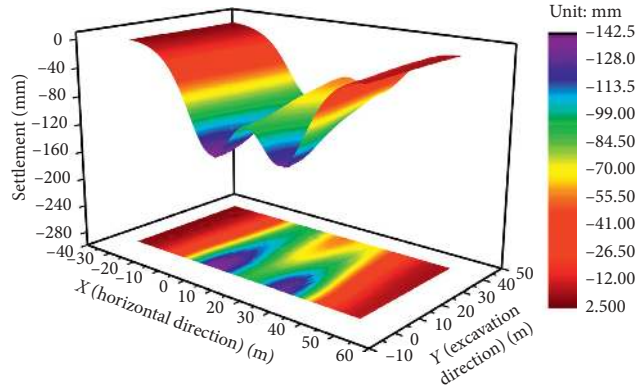

Figure 28: Surface settlement distribution after construction (without grouting).

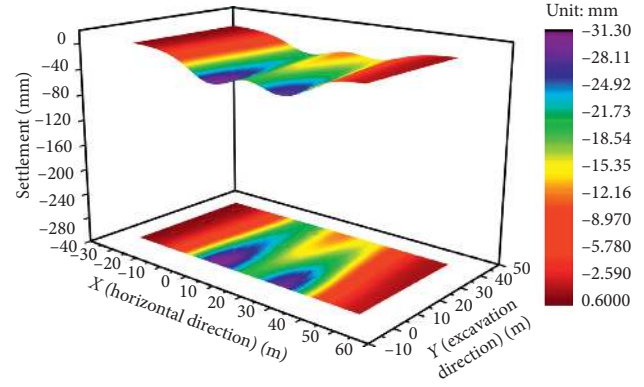

Figure 29: Surface settlement distribution after construction (with grouting).

Section 3.4 can refer to the results of numerical simulation to determine the proportion of each stage.

6. Conclusions

(1) The introduced double slurry pre-grouting obtained remarkable results: the soil mass in the working face was solid and stable after excavation, which can address the common problem of collapse in the past. Erecting a long pipe shed one time instead of building multiple short ones many times reduces the disturbance to the soil so it is safer and more reliable. It is cost-effective to reinforce the bottom of initial support when building loess tunnels in water-rich loess areas.

(2) To control the settlement in time and precisely during the construction process, the total settlement limit should be divided into every process according to similar engineering experience, numerical simulation, and theoretical calculation. The monitoring results show that the settlement of each process is lower than its limit with comprehensive measures.

(3) The settlement of metro tunnelling mainly occurs from excavation to initial support construction, after which the deformation of all measured targets does not change obviously. The self-weight of the building has a negative spillover into adjacent settlement, but its foundation in the soil can resist parts of the effect. The unevenness of deformation in different areas can be addressed through the well-directed support reinforcement.

(4) The finite element method is not accurate in the quantitative calculation and design of underground structures, but it can reflect the trends of construction parameters such as deformation and strain, supposing the definition of construction stage complies with the practical engineering.

Data Availability

The data supporting this research article are available from the corresponding author on request.

Conflicts of Interest

The authors declare that they have no conflicts of interest.

Acknowledgments

The authors gratefully acknowledge the financial support by the National Key R&D Program of China (no. 2018YFC0808706) and the Project on Social Development of Shaanxi Provincial Science (no. 2018SF-378).

References

[1] F. Martos, *Concerning an Approximate Equation of the Subsidence Trough and its Time Factors*, pp. 191–205, International Strata Control Congress, Leipzig, Germany, 1958.

[2] B. Schmidt, *Settlements and ground movements associated with tunnelling in soil*, Ph.D. thesis, University of Illinois, Champaign, IL, USA, 1969.

[3] R. B. Peck, "Deep excavations and tunneling in soft ground," in *Proceedings of the 7th International Conference on Soil Mechanics and Foundations (ICSMFE)*, pp. 225–290, Mexico City, USA, August 1969.

[4] P. B. Attewell and I. W. Farmer, "Ground disturbance caused by shield tunnelling in a stiff, overconsolidated clay," *Engineering Geology*, vol. 8, no. 4, pp. 361–381, 1974.

[5] W. J. Rankin, "Ground movements resulting from urban tunnelling: predictions and effects," *Geological Society*, vol. 5, no. 1, pp. 79–92, 1988.

[6] D. Wu, T. Deng, R. Zhao, and Y. Wang, "THM modeling of ground subsidence induced by excavation of subway tunnel," *Computers and Geotechnics*, vol. 94, pp. 1–11, 2018.

[7] A. Darabi, K. Ahangari, A. Noorzad, and A. Arab, "Subsidence estimation utilizing various approaches-a case study: tehran no. 3 subway line," *Tunnelling and Underground Space Technology*, vol. 31, pp. 117–127, 2012.

[8] K. Ahangari, S. R. Moeinossadat, and D. Behnia, "Estimation of tunnelling-induced settlement by modern intelligent methods," *Soils and Foundations*, vol. 55, no. 4, pp. 737–748, 2015.

[9] S. D. Mohammadi, F. Naseri, and S. Alipoor, "Development of artificial neural networks and multiple regression models for the NATM tunnelling-induced settlement in Niayesh subway tunnel, Tehran," *Bulletin of Engineering Geology and the Environment*, vol. 74, no. 3, pp. 827–843, 2015.

[10] M. Hasanipanah, M. Noorian-Bidgoli, D. Jahed Armaghani, and H. Khamesi, "Feasibility of PSO-ANN model for predicting surface settlement caused by tunneling," *Engineering with Computers*, vol. 32, no. 4, pp. 705–715, 2016.

[11] C. Camós and C. Molins, "3D analytical prediction of building damage due to ground subsidence produced by tunneling," *Tunnelling and Underground Space Technology*, vol. 50, pp. 424–437, 2015.

[12] D. Bouayad, F. Emeriault, and M. Maza, "Assessment of ground surface displacements induced by an earth pressure balance shield tunneling using partial least squares regression," *Environmental Earth Sciences*, vol. 73, no. 11, pp. 7603–7616, 2015.

[13] A. T. C. Goh, W. Zhang, Y. Zhang, Y. Xiao, and Y. Xiang, "Determination of earth pressure balance tunnel-related maximum surface settlement: a multivariate adaptive regression splines approach," *Bulletin of Engineering Geology and the Environment*, vol. 77, no. 2, pp. 489–500, 2018.

[14] L. Cao, D. Zhang, Q. Fang, and L. Yu, "Movements of ground and existing structures induced by slurry pressure-balance tunnel boring machine (SPB TBM) tunnelling in clay," *Tunnelling and Underground Space Technology*, vol. 97, Article ID 103278, 2020.

[15] S. R. Moeinossadat and K. Ahangari, "Estimating maximum surface settlement due to EPBM tunneling by Numerical-Intelligent approach-a case study: tehran subway line 7," *Transportation Geotechnics*, vol. 18, pp. 92–102, 2019.

[16] X. G. Yu, G. H. Xing, and Z. Q. Chang, "Flexural behavior of reinforced concrete beams strengthened with near-surface mounted 7075 aluminum alloys bars," *Journal of Building Engineering*, vol. 31, no. 9, 2020.

[17] S. S. Xu, H. Lei, C. Li, H. Q. Liu, J. X. Lai, and T. Liu, "Model test on mechanical characteristics of shallow tunnel excavation failure in gully topography," *Engineering Failure Analysis*, vol. 119, no. 1, 2021.

[18] Y. Mahmutoğlu, "Surface subsidence induced by twin subway tunnelling in soft ground conditions in Istanbul," *Bulletin of Engineering Geology and the Environment*, vol. 70, no. 1, pp. 115–131, 2011.

[19] S.-L. Shen, H.-N. Wu, Y.-J. Cui, and Z.-Y. Yin, "Long-term settlement behaviour of metro tunnels in the soft deposits of Shanghai," *Tunnelling and Underground Space Technology*, vol. 40, pp. 309–323, 2014.

[20] X.-w. Tang, P.-l. Gan, W. Liu, and Y. Zhao, "Surface settlements induced by tunneling in permeable strata: a case history of Shenzhen Metro," *Journal of Zhejiang University-Science A*, vol. 18, no. 10, pp. 757–775, 2017.

[21] G. Ramos Schneider, A. Garcia-Fontanet, A. Ledesma, R. Raveendra, and T. Polo Orodea, "Toronto-york spadina subway extension tunnelling under schulich building," *Canadian Journal of Civil Engineering*, vol. 46, no. 2, pp. 87–103, 2019.

[22] D. Jin, D. Yuan, X. Li, and H. Zheng, "Analysis of the settlement of an existing tunnel induced by shield tunneling underneath," *Tunnelling and Underground Space Technology*, vol. 81, pp. 209–220, 2018.

[23] B. Duan and L. Li, "Grouting reinforcement technique for subsurface excavation of group metro tunnels construction in complex environment," *Disaster Advances*, vol. 5, no. 4, pp. 1508–1512, 2012.

[24] X. Li and X. Chen, "Using grouting of shield tunneling to reduce settlements of overlying tunnels: case study in Shenzhen metro construction," *Journal of Construction Engineering and Management*, vol. 138, no. 4, pp. 574–584, 2012.

[25] S. Zhou, J. Xiao, H. Di, and Y. Zhu, "Differential settlement remediation for new shield metro tunnel in soft soils using corrective grouting method: case study," *Canadian Geotechnical Journal*, vol. 55, no. 12, pp. 1877–1887, 2018.

[26] Z. F. Wang, S. L. Shen, G. Modoni, and A. N. Zhou, "Excess pore water pressure caused by the installation of jet grouting columns in clay," *Computers and Geotechnics*, vol. 125, Article ID 103667, 2020.

[27] X. Zhang, C. Zhang, and J. Wang, "Effect of closely spaced twin tunnel construction beneath an existing subway station: a case study," *Journal of Testing and Evaluation*, vol. 46, no. 4, pp. 1559–1573, 2018.

[28] Z. Ding, X. Zhang, X. Yin, and J. Jiang, "Analysis of the influence of soft soil grouting on the metro tunnel based on field measurement," *Engineering Computations*, vol. 36, no. 5, 2019.

[29] J. Z. Xiao, F. C. Dai, Y. Q. Wei, Y. C. Xing, H. Cai, and C. Xu, "Analysis of mechanical behavior in a pipe roof during excavation of a shallow bias tunnel in loose deposits," *Environmental Earth Sciences*, vol. 75, no. 4, p. 293, 2016.

[30] J.-D. Yu, Y.-H. Hong, Y.-H. Byun, and J.-S. Lee, "Non-destructive evaluation of the grouted ratio of a pipe roof support system in tunneling," *Tunnelling and Underground Space Technology*, vol. 56, pp. 1–11, 2016.

[31] P. Zhang, B. Ma, C. Zeng, H. Xie, X. Li, and D. Wang, "Key techniques for the largest curved pipe jacking roof to date: a case study of Gongbei tunnel," *Tunnelling and Underground Space Technology*, vol. 59, pp. 134–145, 2016.

[32] Y. Shi, J. Fu, J. Yang, C. Xu, and D. Geng, "Performance evaluation of long pipe roof for tunneling below existing highway based on field tests and numerical analysis: case study," *International Journal of Geomechanics*, vol. 17, no. 9, p. 04017054, 2017.

[33] P. Zhang, S. S. Behbahani, B. Ma, T. Iseley, and L. Tan, "A jacking force study of curved steel pipe roof in Gongbei tunnel: calculation review and monitoring data analysis," *Tunnelling and Underground Space Technology*, vol. 72, pp. 305–322, 2018.

[34] X. Hu, S. Deng, and Y. Wang, "Test investigation on mechanical behavior of steel pipe-frozen soil composite structure based on Freeze-Sealing Pipe Roof applied to Gongbei tunnel," *Tunnelling and Underground Space Technology*, vol. 79, pp. 346–355, 2018.

[35] J. B. Wang, Q. Zhang, Z. P. Song, and Y. W. Zhang, "Experimental study on creep properties of salt rock under long-period cyclic loading," *International Journal of Fatigue*, vol. 143, no. 2, 2021.

[36] J. C. Zhang, Q. X. Yan, M. H. Sun, B. J. Li, W. Y. Chen, and H. Chen, "Experimental study on the vibration damping of two parallel shield tunnels connected by an assembled transverse passage," *Tunnelling and Underground Space Technology*, vol. 107, 2021.

[37] C. Zhang, K. Han, and D. Zhang, "Face stability analysis of shallow circular tunnels in cohesive-frictional soils," *Tunnelling and Underground Space Technology*, vol. 50, pp. 345–357, 2015.

[38] T. Y. Xu, Z. J. Zhou, R. P. Yan et al., "Real-time monitoring method for layered compaction quality of loess subgrade based on hydraulic compactor reinforcement," *Sensors*, vol. 20, no. 15, Article ID 4288, 2020.

[39] Z. J. Zhou, F. Xu, J. T. Lei et al., "Experimental study of the influence of different hole-forming methods on the bearing characteristics of post-grouting pile in Loess Areas," *Transportation Geotechnics*, vol. 26, no. 1, 2021.

[40] J. Lv, X. Li, Z. Li, and H. Fu, "Numerical simulations of construction of shield tunnel with small clearance to adjacent tunnel without and with isolation pile reinforcement," *KSCE Journal of Civil Engineering*, vol. 24, no. 1, pp. 295–309, 2020.

[41] J. Qiu, Y. Lu, J. Lai, C. Guo, and K. Wang, "failure behavior investigation of loess metro tunnel under local-high-pressure water environment," *Engineering Failure Analysis*, vol. 115, Article ID 104631, 2020.

[42] J. B. Wang, Q. Zhang, Z. P. Song, Y. W. Zhang, and X. R. Liu, "Mechanical properties and damage constitutive model for uniaxial compression of salt rock at different loading rates," *International Journal of Damage Mechanics*, vol. 30, no. 1, 2021.

[43] Y. Zhang, Z. Song, and X. Weng, "A constitutive model for loess considering the characteristics of structurality and anisotropy," *Soil Mechanics and Foundation Engineering*, vol. 57, 2020 In press.

[44] Z. J. Zhou, Z. P. Zhang, and C. R. Chen, "Application of load transfer method for bored pile in loess area," *European Journal of Environmental and Civil Engineering*, vol. 24, no. 13, 2020.

[45] H. Wu, Y. J. Zhong, W. Xu, W. Shi, and X. H. Shi, "Experimental investigation of ground and air temperature fields of a cold-region road tunnel in NW China," *Advances in Civil Engineering*, vol. 2020, Article ID 4732490, 13 pages, 2020.

[46] Y. Y. Li, J. Linghu, Z. L. Li et al., "Comparison of durability and mechanism between sprayed concrete and ordinary concrete at different erosion age," *Journal of Materials in Civil Engineering*, vol. 33, no. 1, 2021.

[47] A. Bagherzadeh, B. Ferdosi, J. Nakhaei, and M. J. Nasri, "Numerical analysis of the support system in the transition zone of the Esfahan subway project," *Arabian Journal of Geosciences*, vol. 8, no. 6, pp. 3985–4000, 2015.

[48] M. Sharghi, H. Chakeri, and Y. Ozcelik, "Investigation into the effects of two component grout properties on surface

settlements," *Tunnelling and Underground Space Technology*, vol. 63, pp. 205–216, 2017.

[49] T. Liu, Y. Xie, Z. Feng, Y. Luo, K. Wang, and W. Xu, "Better understanding the failure modes of tunnels excavated in the boulder-cobble mixed strata by distinct element method," *Engineering Failure Analysis*, vol. 116, 2020.

[50] W. Liu, J. Chen, L. Chen, Y. Luo, Z. Shi, and Y. Wu, "Nonlinear deformation behaviors and a new approach for the classification and prediction of large deformation in tunnel construction stage: a case study," *European Journal of Environmental and Civil Engineering*, vol. 24, no. 13, 2020.

[51] E. Moosavi, R. Shirinabadi, E. Rahimi, and M. Gholinejad, "Numerical modeling of ground movement due to twin tunnel structure of esfahan subway, Iran," *Journal of Mining Science*, vol. 53, no. 4, pp. 663–675, 2018.

[52] Z. Zhang, F. Sun, and B. Chen, "Thermo-mechanical coupled analysis for tunnel lining with circular openings," *Tunnelling and Underground Space Technology*, vol. 102, Article ID 103409, 2020.

[53] X. G. Liu, W. P. Zhang, X. L. Gu, and Z. W. Ye, "Probability distribution model of stress impact factor for corrosion pits of high-strength prestressing wires," *Enginerring Structures*, vol. 227, no. 2, 2021.

[54] M. Nematollahi and D. Dias, "Three-dimensional numerical simulation of pile-twin tunnels interaction-case of the Shiraz subway line," *Tunnelling and Underground Space Technology*, vol. 86, pp. 75–88, 2019.

[55] K. Wu and Z. Shao, "Visco-elastic analysis on the effect of flexible layer on mechanical behavior of tunnels," *International Journal of Applied Mechanics*, vol. 11, no. 3, 2019.